20th International Conference on Structural Mechanics in Reactor Technology (SMiRT 20)
Espoo, Finland, August 9-14, 2009
SMiRT 20-Division 8, 2603

A Model to Monitoring Real-time Fracture of Concrete Subjected to the Load from Tendons by AE Technique

Yu-Cheng Kan[a], Kuang-Chih Pei[b], S.-Y. Chen[c], Tsong Yen[d]

[a] *Associate Professor, Chaoyang University of Technology, Taiwan, yckan@cyut.edu.tw*
[b] *Engineers, Institute of Nuclear Energy Research, Taiwan*
[c] *President, FEA-Opt Technology, s-y.chen@fea-optimization.com*
[d] *Professor, Chaoyang University of Technology, Taiwan, yckan@cyut.edu.tw*

Keywords: Fracture, pre-stressed concrete, bearing plate, acoustic emission.

1 ABSTRACT

Acoustic emission technique (AE) to monitor the load test on reinforced concrete structure can reveals more details for the structural integrity. The tendon system results in a distributive pressured state within the concrete of the entire containment wall to prevent fracture due to the inside peak pressure; however, some parts of this system like the anchor – a trumpet type bear plate may cause noticeable concentration load on the concrete. In this research, a small-scaled concrete specimen being embedded with a trumpet bearing plate was designed and fabricated for simulating a bearing system of pre-stressed concrete. The AE technique was applied to record/monitor the emitted ultrasonic wave in the specimen during load test being performed in a MTS system. The obtained hit-count history profiles (vs. time or load), will be observed and discussed in this paper. A finite element analysis, based on ANSYS code, was also conducted to predict the failure of concrete around a trumpet plate as an anchorage system of pre-stressed concrete structure. The result of analysis was found consistent with the test results.

2 INTRODUCTION

Recently, the issue of extension or renew of the service life of nuclear power plant attracts more and more concerns due to its low-carbon emission feature. Hence, the techniques to evaluate the applicability and to replace the parts of the power plant become more significant. As far as the pre-stressed concrete containments (PCCs) is concerned, the U.S. Nuclear Regulatory Commission has been issuing this information notice to alert addressees to degradation of PCC. The specific items addressed are (1) pre-stressing tendon wire breakage, (2) the effects of high temperature on the pre-stressing forces in tendons, and (3) trend analysis of pre-stressing forces. It is expected that recipients will review the information for applicability to their facilities and consider actions, as appropriate, to avoid similar problems.

2.1 Degradation of pre-stressed concrete

Pre-stressed reinforced concrete (PRC) containment with post-tension system design is mostly used for nuclear power plant with pressurized water reactor system (PWR) to prevent concrete fracture due to the inside peak pressure. The post-tension system results in a distributive pressured state within the concrete of the entire containment wall; however, some parts of this system like the trumpet anchor bearing system may cause stress concentration in the concrete around this area.

As nuclear power plants continue to age, in particular, plants with a PCC, the management and mitigation of effects of degradation as a result of aging become increasingly more important. The containment structure serves as the final barrier against the release of fission products to the environment under postulated design-basis accident conditions. Therefore, it is essential that its integrity to be maintained. Focus on the pre-stressing tendon system for containment integrity is based on the vital role it plays.

PCC degradations, such as concrete splitting, water infiltration into tendon galleries, and concrete

cracking in the containment, all affect the containment's ability to function properly. It remains important to ensure that the cumulative effects of degradation mechanisms do not compromise the safety of the containment. The attributes discussed in the three attachments will be useful in identifying the potential problem areas and in evaluating the results of the in-service inspections of containments.

2.2 Acoustic emission applying to concrete

Acoustic emission monitoring was first formulated by Obert (1941) and Hodgson(1942), who applied the technique in predicting the rock bursts in mines, generating during the excavation process. Kaiser (1953) discovered an irreversible characteristic of AE signals, called Kaiser effect in metals. Recently, the AE technique has been used extremely as a monitoring tool for metallic structures in nuclear, chemical and aerospace industries.

The earliest application of AE in concrete was performed by Robinson (1965) who studied AE in the range of 13-14 kHz in mortar and concrete cubes with various amounts and sizes of aggregates. His results revealed that AE technique can provide an earlier detection of structural change than that of convectional methods. Wells (1970) conducted a similar experiment and observed that noise emission starts somewhere over 50 percent ultimate strength and increases as the failure load is approached. Rossi (1994) applied the acoustic emission in fracture mechanics of concrete and creep of concrete to detect the propagating of micro-cracks. Kan and Pei et al. (2007) monitored the acoustic emission signals of a reinforced concrete slab under a load test and revealed a crack incubation phenomenon which can be referred to as the Kaiser effect. It has also found that an increasing amount of research and practice dealing with the AE technique being conducted on concrete structures.

3 EXPERIMENTAL PROGRAM

The experiments of this research used a specific designed concrete cube embedded with a scaled trumpet bear plate. The preparation and test works are mentioned as following:

3.1 Material preparations

3.1.1 Cement

The cement used in the concrete construction project of the power plant is Type II Portland cement which performs moderate sulfate resistance and is the only kind used for the entire experiment following the ASTM C595 for concrete with minor sulfate resistance; the cement performance is suitable for concrete structures in marine environment or seashore.

3.1.2 Aggregate

Crushed limestone is adopted in concrete as coarse aggregate with a maximum particle size of 10 mm. The fine aggregate has a fineness modulus of 2.53, according to ASTM C136. The specific gravities of coarse aggregate and fine aggregate are 2.65 and 2.62, respectively, measured following the ASTM C127 and ASTM C128. The strength and toughness of concrete are thought being dominated significantly by the texture and strength of the aggregates.

3.1.3 Mixture of Concrete

A concrete mixture designed in this research is shown in Table 1. The water-to-cement ratio of the mixture is 0.65. An admixture super-plasticizer complying with ASTM C 494 was employed in the mixture. It was used to improve the workability in fresh concrete stage.

Table 1 Mixture of concrete

Component	Weight (kg / m^3)
Water	228
Cement	350
Sand	841
Aggregate	835
Super-plasticizer	4.20

3.2 Testing Specimens

In this testing program, two pieces of identical specimens were specifically designed and cast using the above concrete mixture. The Φ10 cm x 20 cm cylinders were used to determine the compressive strength. The compressive strength of the mixture at 14 days is about 21.0 MPa. The test specimen of 30 x 30 x 30 cm in dimension with a trumpet bear plate emended in the bottom face was fabricated to simulating the anchorage end of the pre-stressed tendon system, as shown in Figure 1. A plastic tube was hooked up onto the hole of the trumpet. In addition, the reinforcements around the trumpet were also placed in the cube according to a design of pre-stressed concrete containment structure.

Figure 1 Profil n

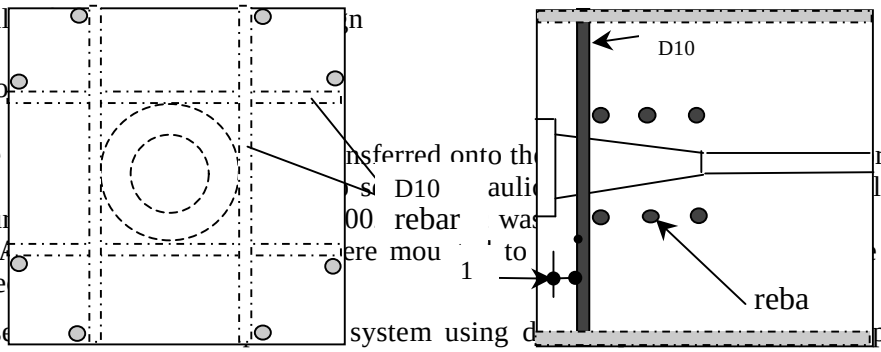

3.3 Testing pro

The procedure nsferred onto th re-stressed concrete. The specimen s D10 aulic lacement control, as shown in Figu 00 rebar wa During the loading process, four A ere mou to specimen. All the signals were re

In this rese system using d ponents of National Instruments Co. and real-time program (LabView7-) was assembled for inspection. The system can continually reco Hz/16bit) emissions over the entire load test (up to 4 hours). The obtained binary counted for later analysis. In this research, the sensor with 40db Integral Preamp function and 500kHz spectral response range (150kHz Max.) was used. Emissions with freque 10k~140kHz were mainly concerne The sensor distribution are shown in Figure 2(b).

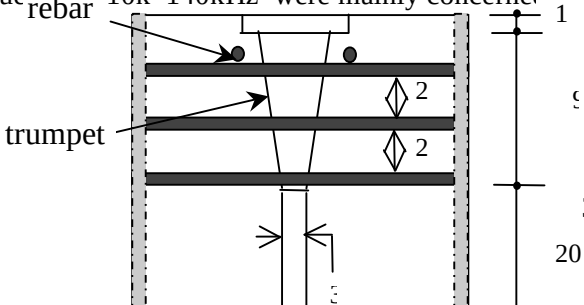

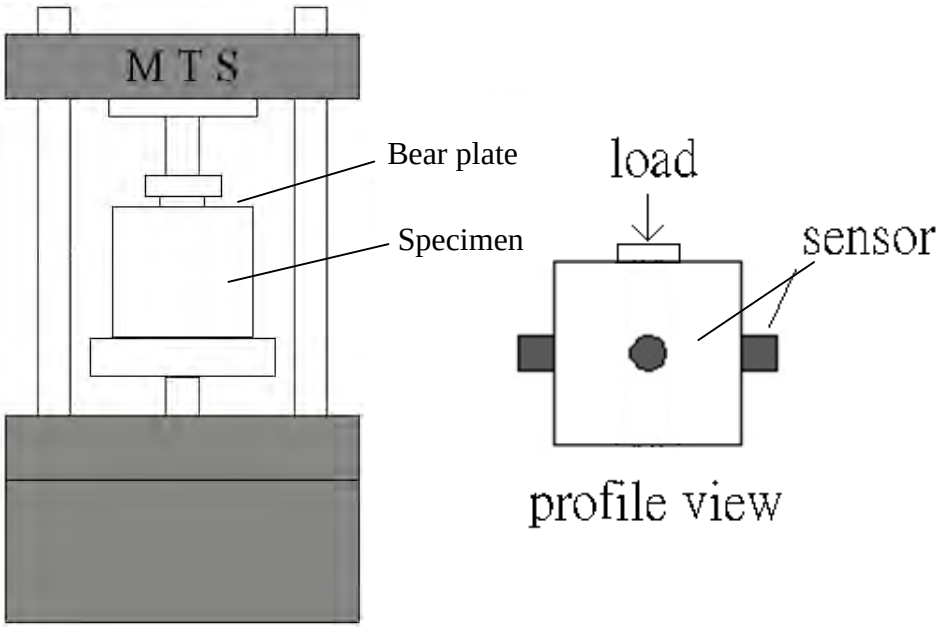

(a) MTS loading system (b) Allocation of AE sensors

Fig. 2 A schematic configuration of loading and AE monitoring system

4 RESULTS AND DISCUSSIONS

4.1 Load test and AE signal Analysis

AE monitoring for two RC specimens will be presented and discussed in this section. Specimen A was the control group, which had been treated in normal air curing. Specimen B had been pre-loaded up to 47 tons after two weeks air-curing. According to the real-time AE monitoring during the pre-loading, we noted that minor cracks occurred inside of the specimen but no major or burst damage happened. After pre-loaded, Specimen B was kept in curing for another 18 days till the final loading test. However, material defects already existed.

Specimen A : (control group)

In this case, loading test lasted 620 seconds with an ultimate load 53.48 tons (F_u at 544 sec.). The corresponding displacement at the load cell (center of bear plate) was 2.72mm. Counting the oscillatory acoustic signals with amplitude over preset thresholds (35mV for sensor 1,3 and 4; 45mV for sensor 2) by second for the whole test, we can statistically plot the monitoring results as the signal density diagram over the entire loading history (see Fig.3). In this figure, four colored lines represent the counted data form

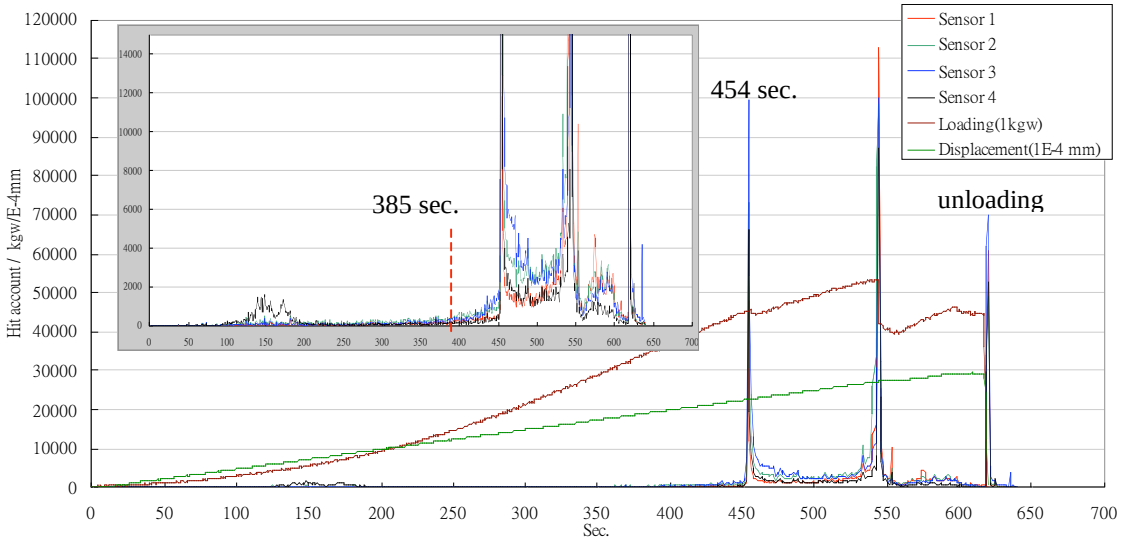

Fig.3 AE signal density diagram for Specimen A under loading test

different sensors, as well as two lines for loading and displacement scaled in *kgw* and 10^{-4}mm respectively. In Fig.3, three burst emissions appear. The peak at 454 sec. was caused by a major cracking event in concrete; the second but highest peak at 544 sec. was the count result from the final breakage. The peak at 620 sec. was due to the MTS unloading, which can be used to synchronize experiment systems as the ending time.

To compare the trend of AE signal densities with the real mechanical performance of specimen, we analyzed not only the densities in Fig.3 but also the hit count accumulative values in the early period of the loading test (see Fig.4). Since the hit count of cracking/opening event relates to the energy released in that event, the accumulation might be referable in quantifying the damage size and its development. In Fig.4, the accumulations grew non-linearly (or exponentially) after 288 sec. when the load was over 19.7 tons ($0.37F_u$) with a displacement 1.43mm. After 385 sec., the loading gradually increased over 34.54 tons ($0.65F_u$) with 1.91mm in displacement, but the accumulative counts increased rapidly. At 454 sec., major cracking event occurred; the load was 45.43 tons ($0.85F_u$) and the load cell went downward 2.26mm. This burst emission might start a new fracture stage. After 454 sec., even though the MTS was still under the displacement-controlled loading process, AE density shown in Fig.3 became larger and more chaotic because of the major loss in concrete integrity. Visible cracks on the specimen surfaces were enlarging till the final rupture.

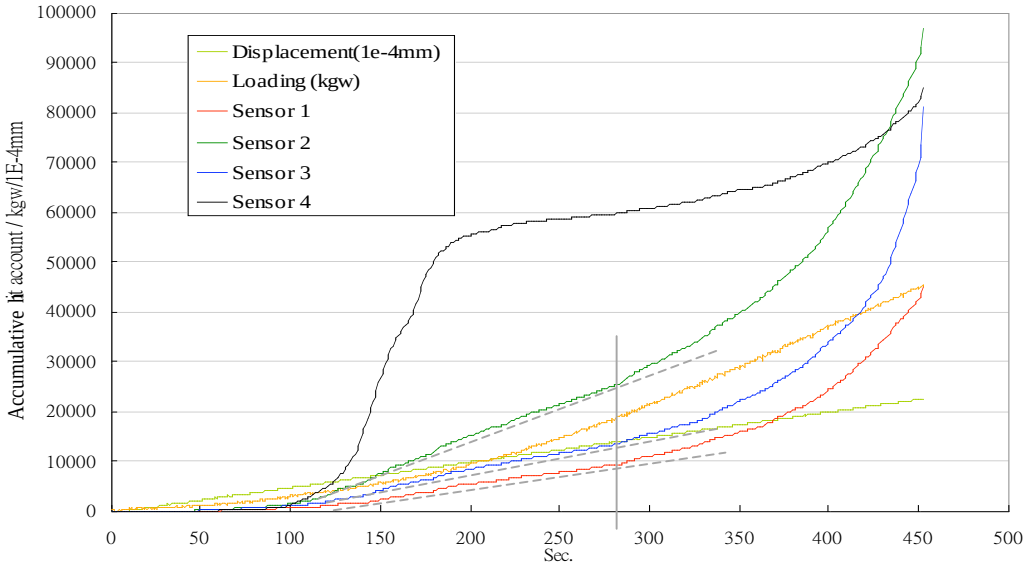

Fig.4 The accumulative hit count values from 0 to 453 sec.

When the specimen was still in good integrity, maximum compression and tension stresses usually occurred under the bear plate or near the trumpet. Crack typically starts at the area with high tension and extend outward. Fig.5(a) presents a crack been found adjacent to the trumpet where noticeable tension stress might exist during the loading. In Fig.4, linear performance before 288 sec. might be a sign of an early fracture stage that the embedded cracks opened, extended, or distributed gradually but did not reach or cross the re-bars yet. When the cracks extended to the re-bars, de-bonding between concrete and re-bar could speedily increase AE signals and stop the earlier linear performance. Following the de-bonding, rubbing between the different material surfaces created more acoustics in a considerable quantity, and would remain from 385 sec. to the end of test. During this period, re-bars became the major support to constrain the specimen against split fracture.

In this case, the existence of inner crack was identified; the embedded cracking events were also pointed out using AE technique. However, no evidence shows that the inner cracks created in the early stage of loading (before 385 sec.) were the same cracks causing the specimen failure. The extension of cracks on the concrete surfaces could be observed in the test but also gave the above question. We noticed that the first visibly cracking at 454 sec. extended upward from the central part of bottom edge through the specimen surface with sensor #3. This crack continually enlarged till 544 sec., and closed when the loading was finally removed. Referring the design of specimen, we noted that the crack enlargement was fully controlled by the three-bars row, and the control had not been failed. The visible cracks of final fracture (544 sec.) also extended upward from the bottom surface (under the three-bars row) but went through the different sides with sensor #2 and #4. These cracks remained opening up to 1mm in width even after unloading, crack-control seemed failed for this direction (see Fig.5(b)).

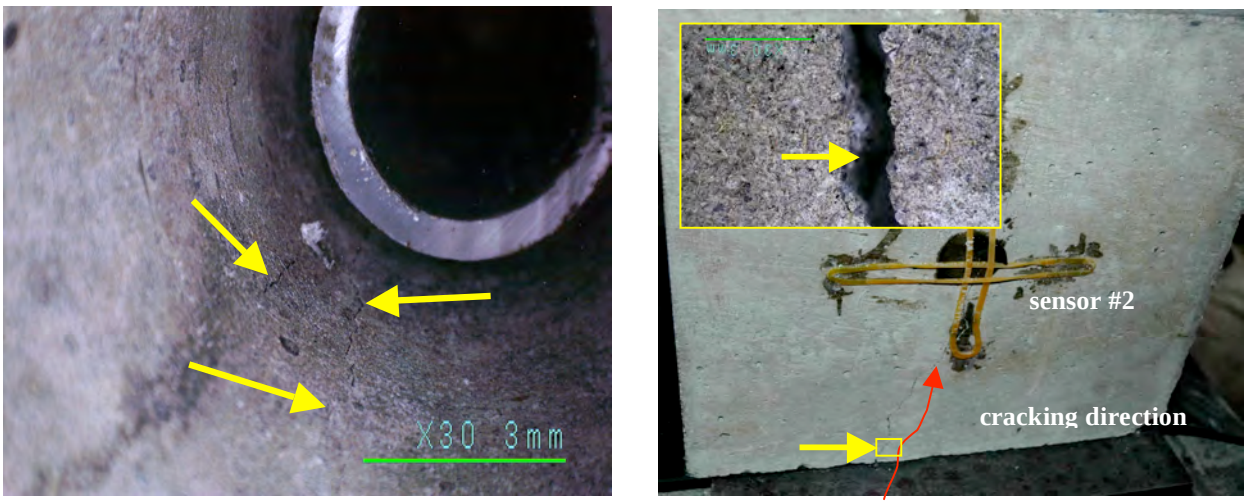

(a) Split cracks near the trumpet (b) Final cracks on the bottom and side surface

Fig. 5 Cracks of specimen after failure

Specimen B : (pre-damaged group)

In case B, loading test lasted 639 seconds with an ultimate load 52.08 tons (F_u at 609sec.). The corresponding displacement near the bear plate center was 2.78mm. The monitoring results from four AE sensors can be plotted as the signal density diagram over the entire loading test (see Fig.6, the preset thresholds: 35mV for sensor 1,3 and 4; 45mV for sensor 2). The colored lines in Fig.6 represent the results form four sensors, as well as two lines for the loading and displacement. In Fig.6, two peak values and two burst emissions are noticeable: the peaks at 445 and 490 sec. were caused by two large cracking events (but not major ones) in concrete; the specimen was finally broken with rupture signals making the highest peak at 610 sec.; the peak at 639 sec. was caused by the MTS unloading.

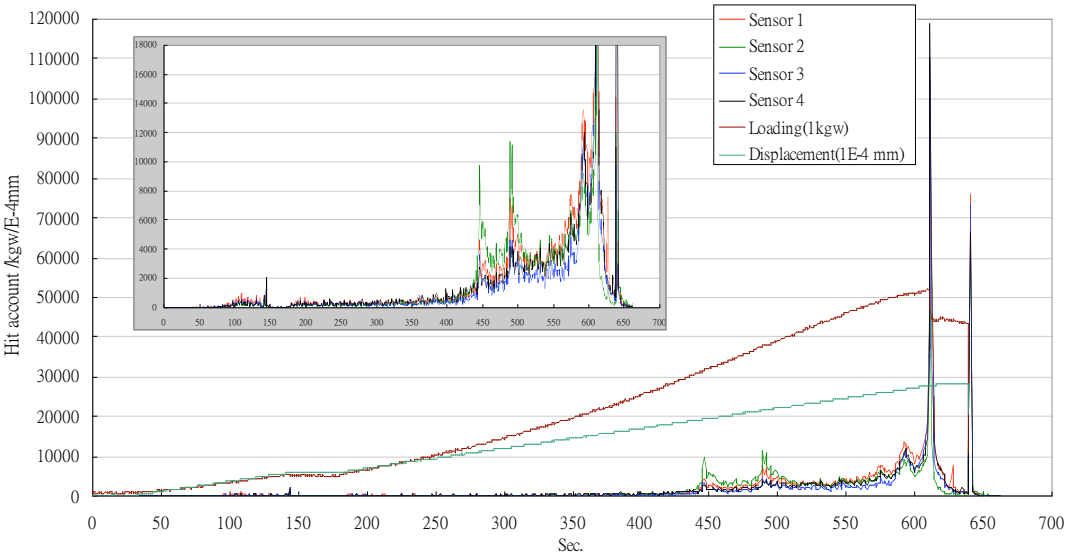

Fig.6 AE signal density diagram for Specimen B under loading test

Like the first case, we analyzed the hit count accumulative values (before 445 sec.) charted in Fig.7. In this figure, the accumulations grew non-linearly after 300 sec. when the load was over 14.5 tons ($0.28F_u$) with a displacement 1.22mm. After 350 sec., the loading steadily increased over 20 tons ($0.4F_u$) with 1.91mm in displacement, but the count accumulation increased rapidly. At 445 sec., a large cracking event happened; the load was 31.64 tons ($0.61F_u$) and the load cell displaced downward 1.94mm. The second noticeable event occurred at 490 sec.; the load was about 38 tons ($0.73F_u$) and the cell moved 2.17mm. The signal density contour of the final breakage was not sharp like the first case (see Fig.6). At least two large

events occurred within 30 sec. period before the final breakage. We also noted that the signal density after 445 sec. went high; large events occurred (see Fig.6), but no visible crack was observed in-site till the final rupture.

Specimen B had been pre-loaded to build minor defects inside. These minor defects certainly reduce the strength of the specimen, but may enhance material toughness (lower the brittleness). Comparing the two

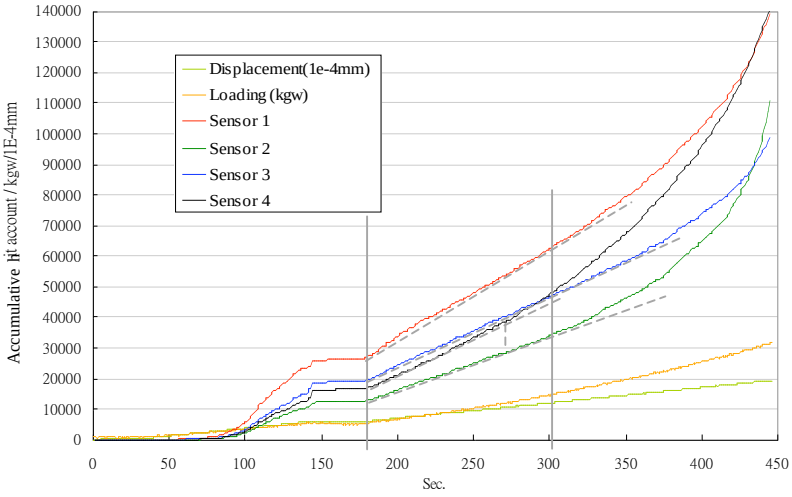

Fig.7 The accumulative hit count values from 0 to 444 sec.

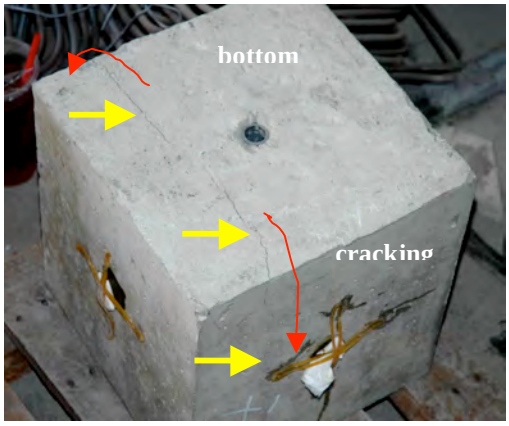

Fig.8 Final cracks on the bottom and side surface

tests, we noted that the linear performance in Fig.7 was under $0.28F_u$, lower than the $0.37F_u$ in specimen A. We also noticed that the large cracking events in case B happened at loads ($0.61F_u$ and $0.73F_u$) lower than the major event in case A. These situations were surely due to the defect concrete. However, the significant events in this case were smaller and flatter than the major one (at 454 sec.) in the first case, and no visible cracks happened after these events. We may assume that specimen B was tougher than specimen A. The small cracks/defects produced by pre-loading might resist the sudden brittle failure.

The visible cracks of final fracture (610 sec.) extended upward from the bottom surface (under the three-bars row) through the side surfaces with sensor #1 and #3 (see Fig.8). These cracks might extend along the three-bars row and crossed or spited the specimen.

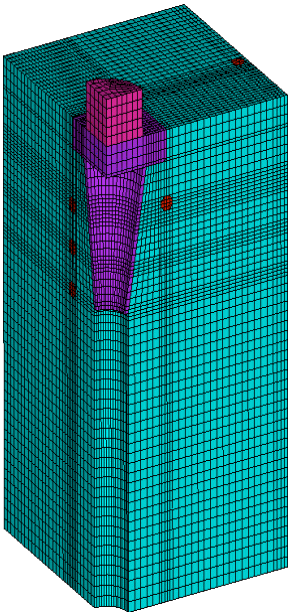

4.2 Numerical analysis

To confirm the experiment by elastic theory, we introduced Finite Element Method (FEM) to describe the static stress distribution within the specimen before major cracking. Because concrete strength in tension is about 10% of the strength value in compression, cracking usually occurs in the area with higher tension stress. Therefore, locating the area with maximum or higher tension stress can puzzled out the mechanism of crack initialization. In this study, ANSYS was used

with an 8-node solid element mesh (see Fig.9, 101393 nodes, 96449 element, iso-parametric). The specimen is symmetric, quarter model used to save computation. The material properties of concrete and re-bar were assumed elastic linear material for simplifying our model. To approach the real boundary condition for the specimen under loading test, the interface between concrete and bear plate/ trumpet is contact situation. The FEM simulation included not only the concrete domain but also the load cell, bear plate, trumpet and re-bars.

Fig.10(a) presents the first principle stress distribution within the concrete domain. We noted that the maximum tension stress occurred near the corner adjacent to the bear plate; this stress may cause burst open or separation. We also found some noticeable tension existing near the lower part of the trumpet. Split may be initialized there. In Fig.10(b), the maximum principle stress distribution (compression due to the loading) was shown. Since the specimen was symmetric, the stresses in X and Y-direction graphed in Fig.10(c) and 10(d) respectively were helpful to confirm the experiments. In these figures, the maximum X- and Y-direction tension stresses occurred near the trumpet, just like the location shown in Fig.5(a). We also found some noticeable Y-direction tensions occurred near the re-bars row in Fig.10(d). These tensions do have the potential to separate the concrete through the re-bars row, just like the final breakages in our tests.

Fig.9 FEM mesh

Fixed in All DOF

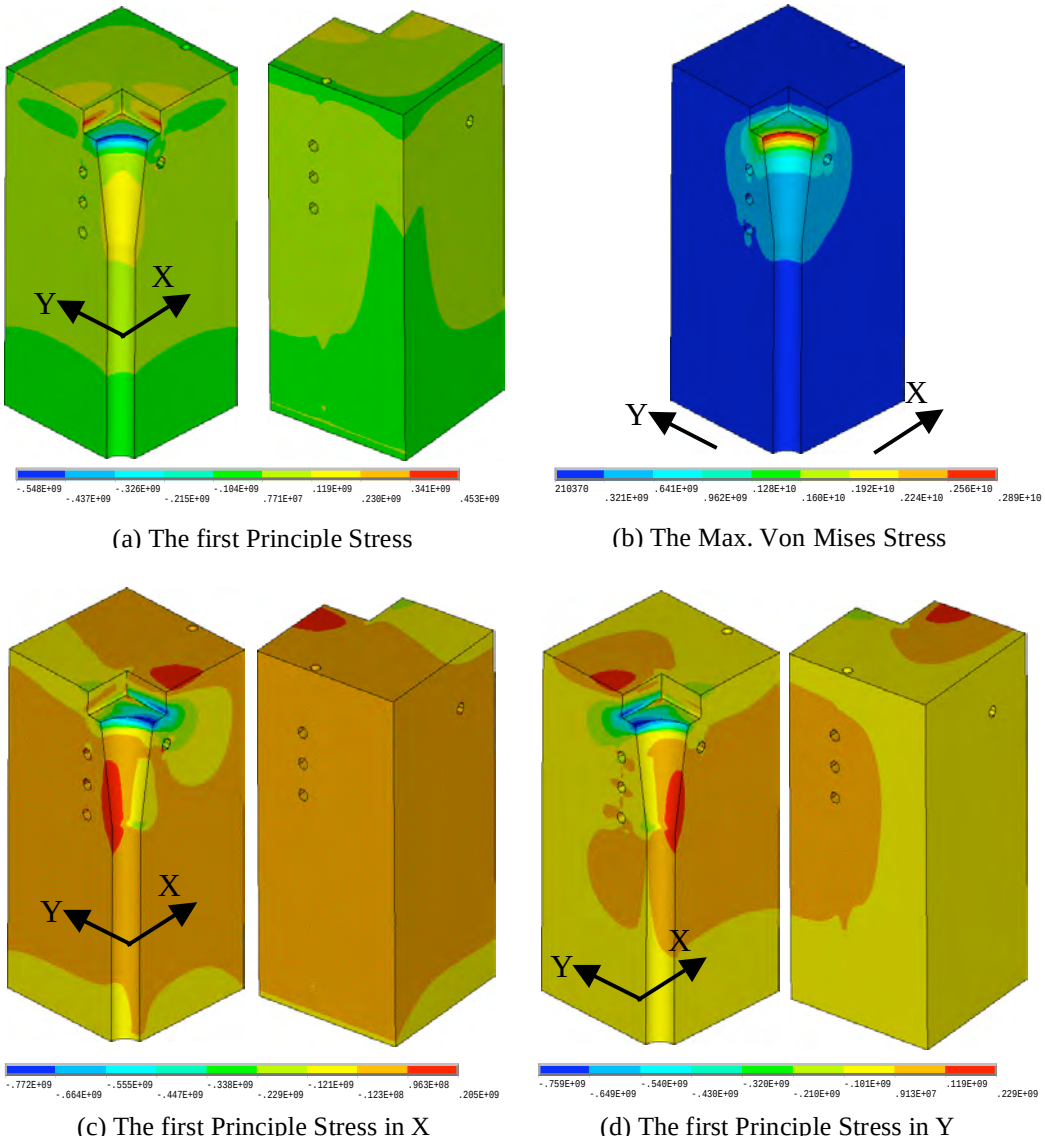

(a) The first Principle Stress (b) The Max. Von Mises Stress

(c) The first Principle Stress in X (d) The first Principle Stress in Y

Fig.10 Finite element analysis of stresses under loading

5. Conclusions

This study investigated and analyzed the AE signals under a load applied on the bear plate simulating a trumpet anchorage end of pre-stressed concrete. According to the AE monitoring experiment and FEM

analysis, the result explored that (1) the inner cracks initiate and extend in early stage of loading (less than $0.4F_u$); (2) the re-bars can constrain but can not limit the enlargement of the inner cracks; (3) the existence of inner cracks may cause the stress re-distribution. In addition, from the FEM analysis and the observation from the specimen cracking type at failure, it revealed that a splitting crack surface apt to take place across the three rows of re-bars. This implies a significant design concern about the conventional arrangement – multi-layers of reinforcements embedded in the bottom mat of a concrete containment structure, which might lead to crack as being subjected to higher stresses. A full scaled mock-up test specimen will be designed and tested based on the results and findings obtained from this research.

REFERENCES

Ober, L. 1941. Use of subaudible noises for prediction of rockbursts. US Bureau of Mines Report 3555.
Hodgson, E. A. 1942. Bull Seismol. Soc. Amer. Vol 32:249.
Kaiser, J. 1953. Knowledge and research on noise measurements during the tensile stressing of metals. Arkiv. Fur Eisenhutten-wesen. Vol. 24:43.

Rossi, P., N. Godart, J. L. Robert, J. P. Gervais and D. Bruhat. Investigation of the basic creep of concrete by acoustic emission. Materials and Structures. Vol 27 P. 510-514.

Robinson, G. S. 1965. Methods of detecting the formation and propagation of micro-cracks in concrete. Proceedings of international conference on structure of concrete and its behaviour under load. London. P131-145.

Wells, D. 1970. An acoustic apparatus to record emissions from concrete under strain. Nuclear Engineering and Design. Vol 12. May. P 80-88.

Kan, Y.-C., K.-C. Pei and D.-W. Lin. 2007. Monitoring the Real-time Fracture within Reinforced Concrete Under Load Test Using Acoustic Emission Recording Technique," Proceeding. **SMiRT-19**, Toronto, Canada, Paper no. G06-5, August 12-17.